MICROTEXTURED RESONATORS FOR MEASURING LIQUID PROPERTIES

Stephen J. Martin[1], Gregory C. Frye[1], Richard W. Cernosek[1], and Stephen D. Senturia[2]

(1) Microsensor Research and Development Department
Sandia National Laboratories, Albuquerque, New Mexico 87185-0351

(2) Department of Electrical Engineering and Computer Science
Massachusetts Institute of Technology, Cambridge, MA 02139

ABSTRACT

The response of smooth- and textured-surface thickness-shear mode (TSM) quartz resonators in liquid has been examined. Smooth devices, which viscously entrain a layer of contacting liquid, exhibit a response that depends on the product of liquid density and viscosity. Textured-surface devices, with either randomly rough or regularly patterned features, also trap liquid in surface features, exhibiting an additional response that depends on liquid density alone. Combining smooth- and textured-surface resonators in a monolithic sensor enables simultaneous extraction of liquid density and viscosity.

INTRODUCTION

A TSM resonator typically consists of a thin disk of AT-cut quartz with circular electrodes patterned on both sides (Fig. 1). Due to the piezoelectric properties and crystalline orientation of the quartz, the application of a voltage between these electrodes results in a shear deformation of the crystal. The crystal can be electrically excited into several resonant modes, each corresponding to a unique standing shear wave pattern (eigenmode) across the thickness of the crystal. The fundamental thickness-shear mode is shown in Fig. 1. For each of these modes, displacement maxima occur at the crystal faces, making these devices sensitive to surface mass accumulation and contacting fluid properties.

A major obstacle to adapting piezoelectric resonators to liquid sensing applications arises from mechanical damping by the liquid medium. Resonators with a surface-normal displacement component generate compressional waves in the contacting liquid. This causes acoustic energy to be radiated away, leading to severe resonance damping. Thickness-shear modes, with only in-plane surface displacement, suffer much less acoustic coupling to a contacting liquid and a tolerable amount of resonance damping.

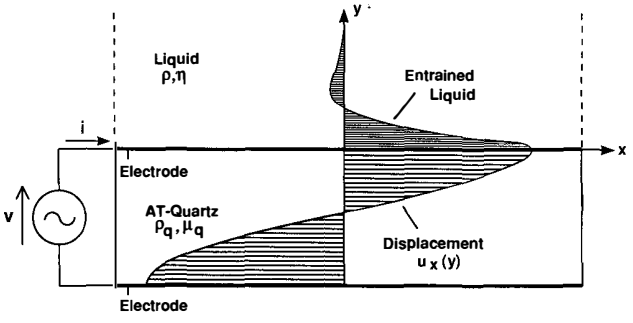

Fig. 1. Cross-sectional view of a smooth TSM resonator with the upper surface contacted by a liquid. Shear motion of the smooth surface causes a thin layer of the contacting liquid to be viscously entrained.

Oscillator circuits have been designed for the TSM resonator that overcome the damping contributed by low viscosity liquids (1). Since the mass sensitivity of the resonator is nearly the same in liquids as in air or vacuum, the device can be used as a sensitive solution-phase microbalance (2). In addition, the sensitivity of the TSM resonator to contacting fluid properties enables it to function as a monitor for these properties. Kanazawa and Gordon (3) have shown that the TSM resonant frequency decreases with liquid immersion as $(\rho\eta)^{1/2}$, where ρ and η are liquid density and viscosity, respectively. Muramatsu *et al.* (4) demonstrated that resonance damping also increases as $(\rho\eta)^{1/2}$. Martin *et al.* (5) derived an equivalent-circuit model to describe the electrical behavior of the TSM resonator in terms of the contacting fluid properties.

This paper will describe the mechanical interactions between smooth- and textured-surface TSM resonators and a contacting liquid. These interactions influence device response in a way that depends on liquid properties, providing a means for measuring these properties.

RESPONSE WITH A SMOOTH SURFACE

When a smooth TSM resonator is operated in contact with a liquid, the shear motion of the surface couples to the contacting liquid, radiating a critically-damped shear wave into the liquid, as shown in Fig. 2a. The decay length δ of this shear wave is (3):

$$\delta = \left(\frac{2\eta}{\omega\rho}\right)^{\frac{1}{2}} \qquad (1)$$

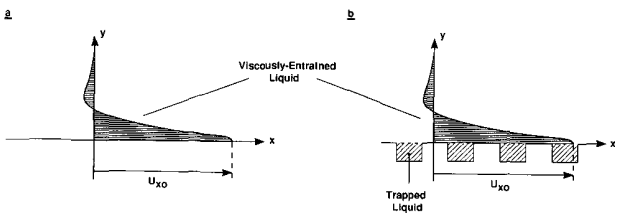

Fig. 2. Cross-sectional view of a resonator surface in contact with a liquid: (a) smooth, showing viscous entrainment, and (b) textured, showing both viscous entrainment and trapping.

0-9640024-0-X/hh1994/$20©1994TRF
DOI 10.31438/trf.hh1994.52

where ω is angular frequency ($2\pi f$). For reference, $\delta = 0.25$ μm in water at 20°C when $f = 5$ MHz. The liquid entrained by the oscillating smooth surface undergoes a progressive phase lag with distance from the surface and is described as "viscously coupled."

Liquid entrainment leads to energy storage and power dissipation in the contacting liquid and affects resonator response. An equivalent circuit model can be used to describe the electrical response of the dry or liquid-contacted resonator (Fig. 3). This modified Butterworth-Van Dyke circuit (6) consists of a "static" capacitance C_o^* (includes any parasitic capacitance) in parallel with a motional branch (L_1, C_1, R_1, L_2, R_2, and L_3). The static capacitance arises between electrodes across the insulating quartz. The motional impedance is due to electrical excitation of a shear-mode mechanical resonance in the piezoelectric quartz. Liquid coupling to the surface modifies this motional impedance. For a smooth surface, viscous coupling introducing a motional inductance (L_2) and a resistance (R_2). These are related to the density ρ and viscosity η of the contacting fluid (5,7):

$$L_2 = \frac{N\pi}{4K^2\omega_s C_o}\left(\frac{\rho\eta}{2\omega_s\mu_q\rho_q}\right)^{\frac{1}{2}} \qquad (2a)$$

$$R_2 = \frac{N\pi}{4K^2 C_o}\left(\frac{\rho\eta}{2\omega_s\mu_q\rho_q}\right)^{\frac{1}{2}} \qquad (2b)$$

where N is the resonator harmonic number (1, 3, 5,...), ω_s is the angular series resonant frequency, while ρ_q, μ_q and K^2 are the quartz density, shear stiffness, and electromechanical coupling factor, respectively. Eqs. 2 are for one-sided liquid contact; for two-sided contact, L_2 and R_2 are doubled. Electrical energy storage in L_2 arises from the kinetic energy of the viscously-entrained liquid layer (with effective thickness δ/2); power dissipation in R_2 arises from shear wave radiation into the liquid.

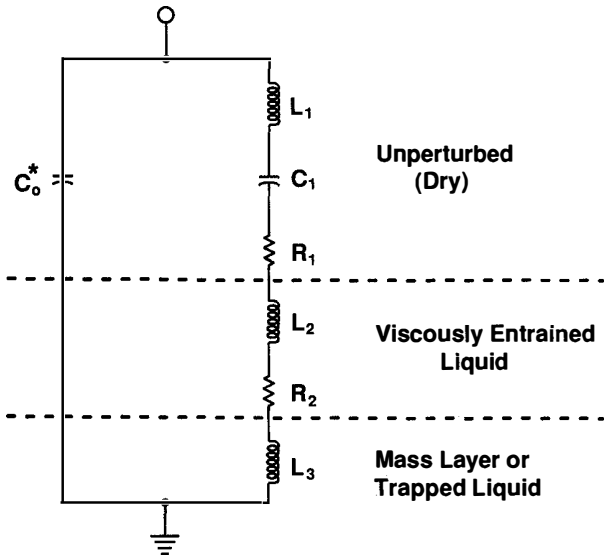

Fig. 3. Equivalent-circuit model to describe the electrical characteristics (for ω near ω_s) of a TSM resonator with liquid loading. Contributions arise from both viscously-coupled liquid (L_2 and R_2) and liquid trapped by surface features (L_3).

The equivalent circuit model in Fig. 3 can be used to derive the changes in series resonant frequency $\Delta f^{(S)}$ and motional resistance $\Delta R^{(S)}$ contributed by viscous coupling to liquid by the *smooth* (superscript *S*) resonator surface (5,7):

$$\Delta f^{(S)} = -\frac{L_2 f_s}{2L_1} = -\frac{2f_s^2}{N\sqrt{\mu_q\rho_q}}\left(\frac{\rho\eta}{4\pi f_s}\right)^{\frac{1}{2}} \qquad (3a)$$

$$\Delta R^{(S)} = R_2 = \frac{\omega_s L_1}{N\pi}\left(\frac{2\omega_s\rho\eta}{\mu_q\rho_q}\right)^{\frac{1}{2}} . \qquad (3b)$$

Eq. 3a is in agreement with Kanazawa and Gordon (3).

Eqs. 2 and 3 indicate that the response of a smooth TSM resonator depends only on the product (ρη) of liquid density and viscosity. Thus, density and viscosity *cannot* be individually resolved from smooth resonator measurements alone.

Response with a Textured Surface

Devices with textured surfaces, either randomly rough or regularly patterned, trap a quantity of fluid in excess of that viscously entrained by a smooth surface (7-9). Vertical features constrain this trapped liquid to move synchronously with the oscillating crystal surface, rather than undergoing a progressive phase lag as occurs with viscously coupled liquid. Thus, this trapped liquid behaves much like an ideal mass layer contributing an areal mass density $\rho_s = \rho h$, where ρ is the liquid density and h, the effective thickness of the trapped liquid layer, is dependent upon the vertical relief of the surface texture.

We can approximate the response of a textured-surface resonator in liquid by separating the solid/liquid interface into two regions, as shown in idealized fashion in Fig. 2b. If we imagine a boundary connecting peaks of the textured surface, then liquid below this boundary is "trapped" and moves synchronously with the surface; liquid above this boundary is viscously coupled (as if by the boundary) and undergoes a progressive phase lag with distance from the boundary.

Liquid trapping by surface texture gives rise to an additional motional impedance element (L_3) in the equivalent-circuit model of Fig. 3 (5,7):

$$L_3 = \frac{N\pi\rho h}{4K^2\omega_s C_o(\mu_q\rho_q)^{1/2}} . \qquad (4)$$

Electrical energy storage in L_3 arises from the kinetic energy of the trapped liquid moving synchronously with the oscillating device surface.

The changes in series resonant frequency and motional resistance arising from liquid contacting a *textured* (superscript *T*) surface are (5,7):

$$\Delta f^{(T)} = -\frac{(L_2+L_3)f_s}{2L_1} = -\frac{2f_s^2}{N\sqrt{\mu_q\rho_q}}\left[\left(\frac{\rho\eta}{4\pi f_s}\right)^{\frac{1}{2}} + \rho h\right] \quad (5a)$$

$$\Delta R^{(T)} = R_2 = \frac{\omega_s L_1}{N\pi}\left(\frac{2\omega_s\rho\eta}{\mu_q\rho_q}\right)^{\frac{1}{2}} . \quad (5b)$$

Response Measurements From Eqs. 5, surface texture is expected to increase the frequency shift caused by liquid contact, in proportion to ρh, without changing the motional resistance. Fig. 4 shows the changes in series resonant frequency Δf and motional resistance ΔR measured vs. the liquid parameter $(\rho\eta)^{1/2}$. Measurements were made using a network analyzer on a smooth and a rough device as water/glycerol solutions contacted one side. The different degrees of surface roughness were obtained by polishing the quartz crystals with various abrasive particle sizes before depositing the conformal Cr/Au electrodes. Surface roughness was quantified using a Wyko RST (Tucson, AZ) profiler (7). The smooth device has an average roughness < 10 nm—much smaller than the liquid decay length δ (250 - 1200 nm for the glycerol solutions tested). For this device, the measured changes in frequency and motional resistance are nearly equal to the predictions for an ideally smooth surface (dashed lines, Eqs. 3). The rough device has an average roughness of 243 nm, comparable to the liquid decay length. Extrapolating the data to $(\rho\eta)^{1/2} = 0$ shows that this device exhibits a large additional frequency shift of approximately 0.87 kHz due to liquid trapping in the randomly-rough surface. From Eq. 5a, this gives h = 150 nm, or roughly 63% of the optically-measured surface roughness. The motional resistance is also slightly larger with the rough device. This indicates increased power dissipation by the rough surface, thought to arise from compressional wave generation by surface asperities (7). For very rough devices, these additional ΔR responses can be significantly larger than those shown in Fig. 4 (7).

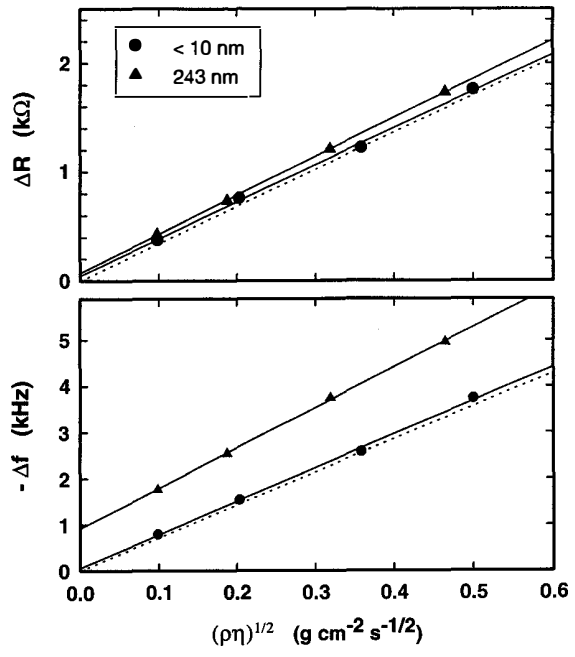

Fig. 4. Change in series resonant frequency (Δf) and motional resistance (ΔR) vs. the liquid parameter $(\rho\eta)^{1/2}$ for TSM resonators with two different surface roughnesses.

Density and Viscosity Extraction

Comparison of Eqs. 3a and 5a indicates that density and viscosity *can* be individually resolved by using a pair of TSM resonators, one smooth and one textured. Since the response due to viscous entrainment of liquid is common to both devices, the difference in response measured upon immersion eliminates this contribution and, in effect, *weighs* the trapped liquid. Subtracting Eq. 3a from Eq. 5a yields the liquid density:

$$\rho = -\frac{N\sqrt{\mu_q\rho_q}}{2f_s^2 h}\left[\Delta f^{(T)} - \Delta f^{(S)}\right] \quad (6)$$

where $\Delta f^{(T)}$ and $\Delta f^{(S)}$ are the frequency shifts measured upon immersion of the textured and smooth resonators. Using Eq. 6 for liquid density, the frequency change of the smooth device (Eq. 3a) is used to determine liquid viscosity:

$$\eta = \frac{2\pi h N\sqrt{\mu_q\rho_q}\,(\Delta f_s)^2}{f_s\left|\Delta f^{(T)} - \Delta f^{(S)}\right|} . \quad (7)$$

Alternatively, if the change in motional resistance $\Delta R^{(S)}$ is measured, liquid viscosity can be determined from this parameter:

$$\eta = \frac{\rho_q\mu_q}{2\omega_s\rho}\left(\frac{N\pi\,\Delta R^{(S)}}{\omega_s L_1}\right)^2 . \quad (8)$$

Monolithic Smooth and Textured Resonator Pair

Fig. 5 shows a monolithic quartz sensor that includes a smooth and a textured TSM resonator to measure liquid density and viscosity. Since these liquid properties (especially viscosity) are temperature dependent, a meander-line resistance temperature device (RTD) is included to measure the liquid temperature. Texture in the form of a surface corrugation is formed on one device by electrodepositing periodic gold ridges on top of the gold electrodes. In order to trap liquid and insure that it moves synchronously with the surface, these ridges are oriented perpendicular to the direction of surface shear displacement (+X crystalline direction).

In fabricating the dual-resonator device, a Cr/Au (30 nm/200 nm) metallization layer is first deposited on both sides of an optically polished AT-cut quartz wafer. This metallization layer is photolithographically patterned to form the resonator electrodes (both sides) and the meander-line RTD (one side). To form a surface corrugation on one resonator, a periodic resist pattern is formed on opposing electrodes. Gold is then electrodeposited, to a thickness of 1.5 μm, onto the electrode between resist strips. When the photoresist is removed, a corrugation pattern remains

with channels approximately 5 μm wide for trapping liquid. Fig. 6 is an SEM micrograph of the sectioned surface, showing the surface corrugation.

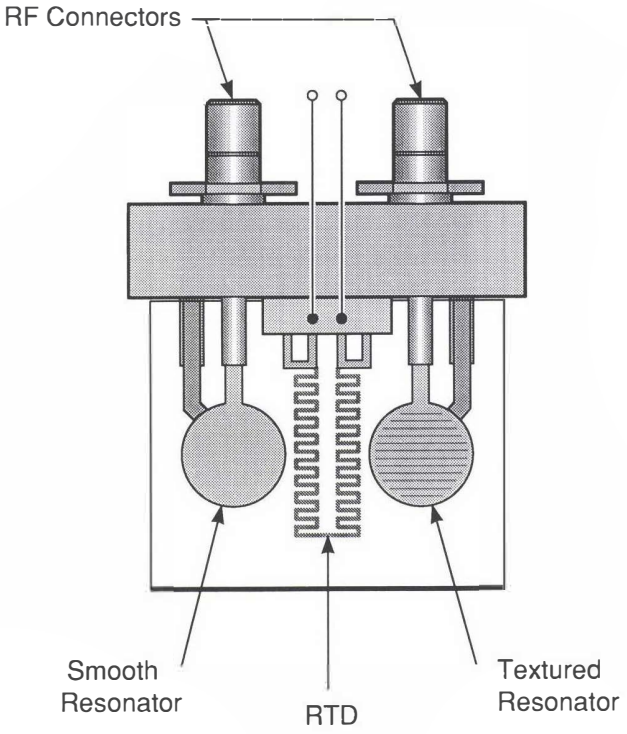

Fig. 5. Monolithic sensor that includes a smooth and textured TSM resonator to measure liquid density and viscosity along with an RTD to measure temperature.

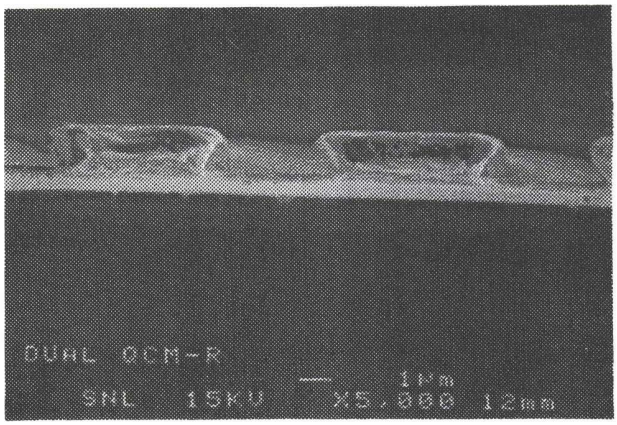

Fig. 6. SEM micrograph of surface corrugation, formed from electrodeposited gold, for trapping liquid at the surface.

An oscillator circuit has been designed to operate the TSM resonator in liquid media and provide outputs indicating the resonant frequency and motional resistance. The oscillator, described by Wessendorf (1), provides an rf output indicating the the series resonant frequency of the crystal, and a dc voltage proportional to the motional resistance $R = R_1 + R_2$. The oscillator circuit will sustain oscillation for motional resistances up to approximately 2 kΩ. Using Eq. 3b, and assuming $\rho = 1$ g/cm^3, this enables resonator operation in liquids with viscosity values up to 34 cP for one-sided contact or 8.6 cP for two-sided contact.

In instrumenting the dual-resonator sensor, each resonator is driven by an independent oscillator circuit. The RF outputs from the oscillators are read by frequency counters while the DC voltages and RTD resistance are read by multimeters. These signals are input to a personal computer. The baseline responses are determined by measuring frequency and motional resistance for each device before immersion. Changes in responses are then measured for the smooth ($\Delta f^{(S)}$, $\Delta R^{(S)}$) and textured ($\Delta f^{(T)}$, $\Delta R^{(T)}$) devices upon immersion. Eqs. 6 and 7 or 8 are then used to determine density and viscosity.

Fig. 7 illustrates the *densitometer function* of the dual-resonator sensor of Fig. 5. The difference in responses $|\Delta f^{(T)} - \Delta f^{(S)}|$ measured between the textured and smooth resonators upon immersion (two-sided liquid contact) is shown vs. liquid density. The response difference is linear with density, despite variations in viscosity between the test liquids. This indicates that liquid trapping is independent of liquid viscosity, as assumed in the simple trapping model outlined above.

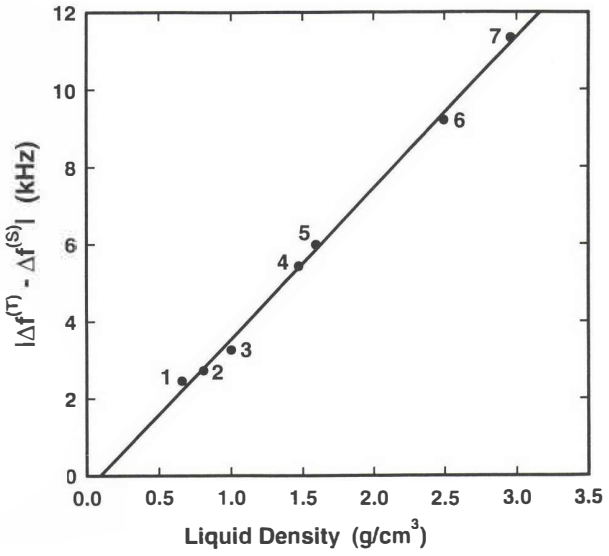

Fig. 7. The difference in frequency changes $|\Delta f^{(T)} - \Delta f^{(S)}|$ measured between the textured and smooth resonators (Fig. 5) upon immersion vs. liquid density. Liquids tested: (1) hexane, (2) butanol, (3) water, (4) chloroform, (5) carbon tetrachloride, (6) dibromomethane, and (7) tetrabromoethane.

Fig. 8 shows a "scatter diagram" that compares liquid densities and viscosities extracted from dual-resonator measurements (circles) with literature values (squares). For $\rho\eta > 0.08$ g^2 cm^{-4} s^{-1} (8 cP-g/cm^3), the crystal is damped too severely to sustain oscillation. This data illustrates that liquid density and viscosity can be extracted from measurements made by a pair of quartz resonators—one smooth and one with surface texture. When compared to the literature values, the average measured density

error in this data set was 5.3% and the average viscosity error was 19.5%.

Interestingly, the points in Fig. 8 divide into density bands according to chemical class: the lowest set (A - J) are hydrocarbons, the middle set (K - M) are chlorinated solvents, while the upper point (N) is a brominated solvent. This data suggest the possibility of identifying pure liquids on the basis of density and viscosity measurements.

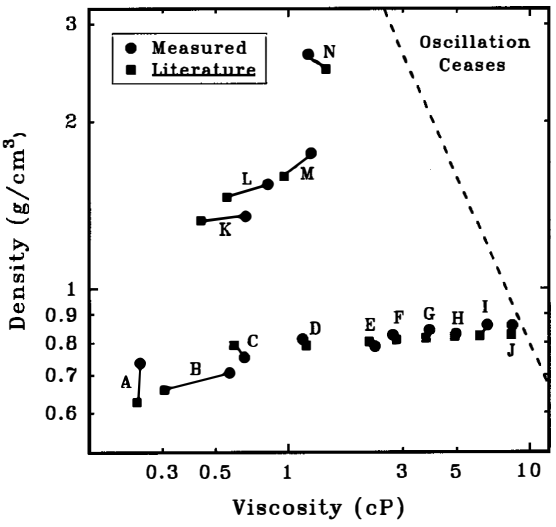

Fig. 8. Scatter diagram comparing the extracted (circles) and literature (squares) values of liquid density and viscosity for organic liquids: (A) n-pentane, (B) n-hexane, (C) methanol, (D) ethanol, (E) n-propanol, (F) n-butanol, (G) n-pentanol, (H) n-hexanol, (I) n-heptanol, (J) n-octanol, (K) dichloromethane, (L) trichloroethylene, (M) carbon tetrachloride, (N) dibromomethane.

CONCLUSION

Quartz resonators with smooth surfaces can be operated in liquids to measure the density-viscosity product of a contacting fluid. Surface texture causes fluid trapping and an additional response proportional to liquid density. Comparing the responses of a pair of resonators—one smooth and one textured—enables liquid density to be extracted. Once density is known, the response of a smooth device yields liquid viscosity.

ACKNOWLEDGEMENTS

The authors wish to thank L. Casaus and K. Rice of Sandia National Laboratories for technical assistance. This work was performed at Sandia National Laboratories, supported by the U.S. Department of Energy under contract No. DE-AC04-94AL8 5000.

REFERENCES

(1) Wessendorf, K. O. *Proc. 1993 Frequency Control Symp.* (IEEE, New York, 1993) pp. 711-717.

(2) Numura, T.; Minemura, A. *Nippon Kagaku Kaishi* **1980**, 1621.

(3) Kanazawa, K. K.; Gordon II, J. G. *Anal. Chem.* **1985**, *57*, 1770-1771.

(4) Muramatsu, H.; Tamiya, E.; Karube, I. *Anal. Chem.* **1988**, *60*, 2142-2146.

(5) Martin, S. J.; Granstaff, V. E.; Frye, G. C. *Anal. Chem.* **1991**, *63*, 2272-2281.

(6) Rosenbaum, J. F. *Bulk Acoustic Wave Theory and Devices*; Artech: Boston, 1988; Sect. 10.5.

(7) Martin, S. J.; Frye, G. C.; Ricco, A. J.; Senturia, S. D. *Anal. Chem.* **1993**, *65*, 2910-2922.

(8) Beck, R.; Pitterman, U.; Weil, K. G. *J. Electrochem. Soc.* **1992**, *139*, 453-461.

(9) Schumacher, R.; Borges, G.; Kanazawa, K. K. *Surface Science* **1985**, *163*, L621-L626.